

# Sources and correction of higher order geometrical distortion for serial MR brain imaging

Mark Holden<sup>a</sup>, Marcel Breeuwer<sup>b</sup>, Kate McLeish<sup>a</sup>, David J Hawkes<sup>a</sup>,  
Stephen F Keevil<sup>a</sup>, Derek LG Hill<sup>a</sup>

<sup>a</sup>Radiological Sciences, Guy's, King's and St. Thomas's School of Medicine,  
Guy's Hospital, London SE1 9RT, UK

<sup>b</sup>EasyVision Advanced Development, Philips Medical Systems,  
Best, The Netherlands

## ABSTRACT

A specially designed phantom consisting of a 3D array of 427 accurately manufactured spheres together with a point-based registration algorithm was used to detect distortion described by polynomial orders 1-4. More than thirty 3D gradient echo (GRE) and multi-slice spin echo (SE) phantom scans were acquired with a Philips 1.5T Gyroscan ACS2. Distortion was measured as a function of: readout gradient strength ( $0.72 \leq G_r \leq 1.7\text{mT/m}$ ), TR/TE/flip angle, shim settings, and temporal distortion change for 11 weekly scans for the FFE sequence and TR/TE/slice gap for SE. Precision measurements for linear distortion were: scale  $\leq 0.03\%$ , shear  $\leq 0.04$  degrees. Linear distortion in the readout dependent directions increased with decreased readout strength ( $r > 0.93$ ). There was a significantly higher ( $p < 0.01$ ) sagittal shear for 5 SE scans compared with 5 FFE ones with the same  $G_r$  - possibly because of slice selection. Different shim settings produced only linear distortion change: up to 2 % scale and 1 degree shear. There was negligible distortion change over time: scale  $< 0.1\%$ , shear  $\leq 0.05$  degrees. There was a decrease in distortion as a function of polynomial order ( $r > 0.9, n = 33$ ), 75% of the distortion was either first or second order.

**Keywords:** serial MR, phantoms, MR geometrical distortion.

## 1. INTRODUCTION

Changes in geometrical distortion have been observed in previous serial MR studies.<sup>1-3</sup> These changes impede the detection of clinically interesting anatomical change. Geometrical distortion mainly arises from  $B_0$  inhomogeneities, errors in the imaging gradients and object susceptibility. Susceptibility effects can be reduced by increasing the readout gradient strength. Previous work on measuring and correcting geometrical distortion for serial MR studies has focussed on scaling error.<sup>1-3</sup> Here we study more general orders such as shears and higher order polynomial terms. For this we used a specially designed phantom.<sup>4</sup> Our main aims were to identify the factors that lead to distortion change and measure temporal variation in distortion. Accordingly we have designed a set of experiments to quantify measurement precision; impact of readout gradient strength ( $G_r$ ), sequence parameters (TR/TE/flip angle) and shim settings on distortion; and distortion change over time. We also aim to determine whether distortion correction can improve the diagnostic quality of brain images. In particular, we have found that different shim settings can lead to changes in scale and shear. Because active shimming involves adjusting gradient currents, it is likely to produce similar effects to changes in calibration of the imaging gradients.

## 2. THEORY

### 2.1. Model of geometrical distortion

In general, geometrical distortion arises because of incorrect frequency encoding. This arises because of: (a) extraneous gradients ( $G'$ ); (b) static field inhomogeneity ( $B_e$ ); (c) chemical shifts ( $\sigma_{cs}$ ); and (d) changes in object susceptibility ( $\chi$ ). Sumanaweera<sup>5</sup> also lists eddy currents, these should be minimal for conventional imaging with modern shielded designs and so we ignore this source. Extraneous gradients,  $G'(x, G_x)$ , may arise because of gradient non-linearities or errors in the gradient strength. Chemical shifts arise because of the shielding effect of surrounding

---

Further author information: D. L. G. Hill: E-mail: Derek.Hill@kcl.ac.uk

electrons.<sup>6</sup> This shielding reduces  $B_0$  by a shielding constant,  $\sigma_{cs}$ .<sup>7</sup> They result in misregistration in the spatial image which is often not considered to be distortion. Changes in object susceptibility,  $\chi(x)$ , modify the effective static field ( $B_0$ ). These sources introduce a phase shift into frequency encoding that can be modelled with the 1D MR imaging equation for a readout line ( $x$ ) with the readout gradient,  $G_x$ .<sup>7</sup> The signal in k-space,  $s(t)$ , is a Fourier transform of the following form:

$$s(t) = \int dx \rho(x, \sigma_{cs}) e^{-j\phi(G_x, G', B_e, \sigma_{cs}, \chi)} \quad (1)$$

Where  $\phi(G_x, G', B_e, \sigma_{cs}, \chi)$  is a phase term related to the distortion sources  $G', B_e, \sigma_{cs}, \chi$  as follows:

$$\phi(G_x, G', \sigma_{cs}, \chi) = \gamma(G_x x + G' x + B_e - \sigma_{cs} B_0 + B_0 f(\chi))t \quad (2)$$

Equation (2) illustrates that the sources introduce perturbations of phase,  $\Delta\phi$ , compared with the undistorted case. This phase shift leads to incorrect frequency encoding and results in misregistration of the spatial signal in the  $x$  (readout) direction (Fourier shift theorem). Notice that only the non-linearities in  $G'$  are likely to be functions of  $G_x$ , so increasing  $G_x$  will reduce the relative contribution of the  $B_e, \sigma_{cs}$  and  $\chi$  terms to the distortion.

Furthermore, since the  $\sigma_{cs}$  and  $\chi$  terms are proportional to  $B_0$  their contribution increases with  $B_0$ . The  $G'$  and  $B_e$  terms are dependent on the imaging system while  $\sigma_{cs}$  and  $\chi$  terms are related to the material that is imaged and its orientation with respect to the readout direction. Consequently, phantom methods can only be used to correct scanner distortion caused by  $G'$  and  $B_e$ .

## 2.2. Measuring geometric distortion

Translations and rotations are unrelated to distortion and are therefore ignored. The components of linear distortion are scale ( $s_x, s_y, s_z$ ) and shear ( $s_{xy}, s_{xz}, s_{yz}$ ). Higher order distortion is described in terms of polynomial coefficients.<sup>4</sup> Given point sets,  $\mathbf{X}$  and  $\mathbf{X}'$  that correspond to undistorted and distorted cases the amount of distortion can be estimated by calculating the mean distance (residual),  $dp$ , between the two sets:

$$dp = \frac{1}{N} \sum_{\mathbf{x} \in \mathbf{X}, \mathbf{x}' \in \mathbf{X}'} |\mathbf{x} - \mathbf{x}'| \quad (3)$$

The  $dp$  residual can be extended to the  $dp(i)$  residual which is a measure of the distortion present after applying transformation,  $\mathbf{T}_i$ , to correct for polynomial order  $i$ :

$$dp(i) = \frac{1}{N} \sum_{\mathbf{x} \in \mathbf{X}, \mathbf{x}' \in \mathbf{X}'} |\mathbf{T}_i \mathbf{x} - \mathbf{x}'| \quad (4)$$

$dp(i)$  can be further extended to give another residual measure,  $dp_4$ , that indicates how much distortion has been detected for each correction order.  $dp_4$  is a 4-tuple measure of the relative change in  $dp$ , for successive polynomial orders, or more precisely:

$$dp_4 = \left( \frac{dp - dp(1)}{dp}, \frac{dp(1) - dp(2)}{dp}, \frac{dp(2) - dp(3)}{dp}, \frac{dp(3) - dp(4)}{dp} \right) \quad (5)$$

The first component of  $dp_4$  indicates how much first order (linear) distortion has been detected, the second component how much second order, and so on.  $dp_4$  provides a concise way of describing the measured distortion for each polynomial order.

## 3. MATERIALS AND METHOD

### 3.1. Phantom and distortion measurement

We use the second version of the head-coil phantom and point-based registration algorithm described elsewhere in this volume<sup>4</sup> (see Figure 7(b) in that paper). The phantom consists of a 3D array of 427 spherical reference structures (hollow spheres) filled with standard copper sulphate contrast agent. The positions of the reference structures are stored and used to measure distortion with a point-based registration algorithm.

**Table 1.** MR sequence details.

identifier	sequence	TR/TE/flip angle	FOV (mm)	num slices	$G_x$ (mT/m)	voxel size (mm)
FFE1	3D GRE	30/4.5/30	256	124	2.55	$1 \times 1 \times 1.8$
FFE2	3D GRE	30/4.5/30	256	110	1.275	$2 \times 2 \times 2$
SE	multislice SE	500/20/90	256	110	1.275	$2 \times 2 \times 2$

**Table 2.** Nomenclature of scans with different sequence parameters.

identifier	GRADIENT ECHO		
	TR (ms)	TE (ms)	flip angle (degrees)
greSTD	30	4.5	30
greTR13	13	4.5	30
greTE3	30	3	30
greTE20	30	20	30
greFA60	30	4.5	60
identifier	SPIN ECHO		
	TR (ms)	TE (ms)	slice gap (mm)
seSTD	500	20	0
seTR200	200	20	0
seTR1000	1000	20	0
seTE40	500	40	0
seGap0.5	500	20	0.5

### 3.2. Experimental data

All scans were acquired using a Philips Gyroscan ACS2 1.5T MR scanner, in the standard birdcage head-coil. Distortion measurements assume that the magnetic field gradients are orthogonal to the static magnetic field. We checked for possible misalignment by extracting the geometry matrix from the scan header, this corresponded to identity matrix to six decimal places indicating negligible misalignment. We therefore write  $G_r \equiv G_x$  without loss of generality. Experiments were performed with both gradient (GRE) and spin echo (SE) sequences; the gradient echo images had two different resolutions. The sequence details are described in Table 1.

### 3.3. Measurement precision

To estimate measurement precision the phantom was scanned six times consecutively with a gradient echo FFE1 sequence. To make this realistic the phantom was repositioned by a few millimetres after each scan.

### 3.4. Sequence parameters

The influence of the sequence parameters was studied with a series of five FFE2 and five SE scans acquired a few minutes apart. The first scan in the series (baseline) was with a standard brain anatomy sequence. The sequence parameters were adjusted to produce a series of scans differing from the baseline by a single parameter. To maximise the effect the parameter was adjusted to either the minimum or maximum permitted value, whichever differed most from the default. The details of the sequence parameters used are shown in Table 2. To compare the distortion in each of the FFE2 scans with respect to the standard one (greSTD) the  $dp$  residual was determined before correction.

### 3.5. Readout gradient strength

According to equation (2) chemical shift misregistration is dependent on the readout gradient strength. Many MR scanners provide a mechanism of compensating for fat/water chemical shift by adjusting the readout gradient strength. For the Philips Gyroscan, the user specifies the desired fat shift in pixels and the scanner calculates the appropriate readout gradient strength. To determine the assigned readout gradient strength the user can enter sequence development mode prior to scan initialisation and access the appropriate record. Hence it is possible to investigate the impact of readout gradient strength on geometrical distortion without adjusting other scan parameters. Five FFE2 scans were acquired consecutively with fat/water shifts adjusted from 1.5 to 3.5 pixels in 0.5 pixel

**Table 3.** Fat/water shift and corresponding readout gradient strength.

fat shift (pixels)	1.5	2	2.5	3	3.5
$G_x$ mT/m	1.7	1.275	1.02	0.85	0.7286

increments, the corresponding readout gradient strengths are shown in Table 3. To assess the overall distortion change as a function of  $G_x$  the  $dp$  residual was found for each scan with respect to the default readout gradient strength ( $G_x = 1.275\text{mT/m}$ ).

### 3.6. Shimming

Shimming refers to the process of reducing magnetic field inhomogeneities. MR scanners are always shimmed during installation, this shim setting is referred to as the default shim (DS). Some small inhomogeneities, however, remain and the Philips Gyroscan provides a method of adjusting the currents in the gradient coils to compensate for these at scan time. The autoshim (AS) procedure refers to automatic shimming optimised over the entire FOV, which is performed immediately prior to scanning. Because MR spectroscopy is very sensitive to field inhomogeneities the Gyroscan also provides a volume localised shim that can be set using the spectroscopy package, this is referred to as the manual shim (MS). Because the shims are set over different volumes they produce different distortion fields. To investigate the impact of different shim settings three FFE1 and three FFE2 scans were acquired with each of the three shim setting, AS, DS, and MS. The MS shim was optimised over a  $1\text{ cm}^3$  cube centred in a spherical reference structure at the middle of the phantom. To assess the change in distortion produced by the different shim settings the  $dp$  residual was determined before correction.

### 3.7. Distortion over time

Temporal variation in distortion was measured with a series of 11 weekly FFE1 scans, the mean (stdev) inter-scan interval was 7 (1) days. Distortion change was measured relative to the first scan.

### 3.8. Higher order distortion

This experiment was designed to investigate how much distortion there was, on average, for each polynomial order. Thirty three scans were acquired with the FFE1, FFE2 and SE sequences. The proportion of each polynomial order was assessed with the mean  $dp_4$ .

### 3.9. Correcting brain images for distortion change

To test this strategy image pairs were acquired of a volunteer and the phantom with the DS and MS shim settings using the FFE1 sequence. The autoshim procedure was found to be unsatisfactory for this purpose as it was not possible to save the shim setting and retrieve it for another scan. Distortion was corrected with respect to the undistorted ball locations ( $\mathbf{X}$ ) and the volunteer images were interpolated with a Hanning-windowed sinc kernel (radius 6 zero crossings). Brain images with the MS shim setting were registered to the DS ones with a mutual information based rigid-body algorithm<sup>8</sup> with and without distortion correction. These were then interpolated with the sinc kernel and subtracted to produce difference images with and without distortion correction. To evaluate the benefit of distortion correction the difference image statistics were calculated using voxels in the sub-dural brain.

## 4. RESULTS

All results are reported with the following coordinate system:  $x$ , the readout direction, is anterior/posterior (A/P),  $y$  is left/right (L/R) and  $z$  is cranio/caudal (C/C or head/foot H/F).

### 4.1. Measurement precision

The precision (stdev) of linear distortion for six FFE1 scans was  $(s_x, s_y, s_z) \leq 0.03\%$  and  $(s_{xy}, s_{xz}, s_{yz}) \leq 0.04^\circ$ , see Table 4. These measurements also indicate a miscalibration of the readout gradient  $G_x$  of  $-1.7\%$  and phase encode gradient  $G_y$  of  $-0.9\%$  and a much smaller one for  $G_z$  of  $-0.15\%$ .

**Table 4.** Precision of linear distortion measurements with respect to the modelled reference structures (absolute) upper table and the detected ones of scan A (relative) lower table.

scan	scale ( % )			shear (degrees)		
	$s_x$	$s_y$	$s_z$	$s_{xy}$	$s_{xz}$	$s_{yz}$
A	98.28	99.09	99.88	0.42	0.41	0.26
B	98.27	99.13	99.82	0.45	0.48	0.27
C	98.28	99.09	99.85	0.39	0.49	0.23
D	98.27	99.13	99.89	0.42	0.40	0.27
E	98.28	99.11	99.83	0.42	0.41	0.24
F	98.26	99.08	99.86	0.42	0.44	0.23
Statistics	$s_x$	$s_y$	$s_z$	$s_{xy}$	$s_{xz}$	$s_{yz}$
mean	98.27	99.11	99.85	0.42	0.44	0.25
std	0.01	0.02	0.03	0.02	0.04	0.02

RELATIVE TO SCAN A						
scan	$s_x$	$s_y$	$s_z$	$s_{xy}$	$s_{xz}$	$s_{yz}$
B	100.00	100.04	99.95	0.02	0.05	0.02
C	99.97	99.99	99.95	-0.03	-0.01	-0.03
D	100.00	100.04	100.02	-0.01	0.00	0.01
E	100.01	100.03	99.94	-0.01	0.03	0.02
F	99.99	100.00	99.98	-0.01	0.01	-0.00
Statistics	$s_x$	$s_y$	$s_z$	$s_{xy}$	$s_{xz}$	$s_{yz}$
mean	99.99	100.02	99.97	-0.01	0.02	0.00
std	0.01	0.02	0.03	0.02	0.02	0.02

**Table 5.** Linear distortion as a function of gradient strength. The target image was the modelled ball positions (absolute).

$G_x$	scale ( % )			shear (degrees)		
	$s_x$	$s_y$	$s_z$	$s_{xy}$	$s_{xz}$	$s_{yz}$
1.7	98.58	99.18	99.91	0.68	0.65	0.36
1.275	98.46	99.12	99.86	0.69	0.84	0.25
1.02	98.24	99.19	99.86	0.77	1.04	0.25
0.85	98.17	99.28	99.89	0.81	1.27	0.25
0.7286	97.87	99.18	99.92	0.94	1.60	0.25
Statistics	$s_x$	$s_y$	$s_z$	$s_{xy}$	$s_{xz}$	$s_{yz}$
mean	98.26	99.19	99.89	0.78	1.08	0.27
std	0.27	0.06	0.03	0.11	0.37	0.05

#### 4.2. Distortion as a function of readout gradient strength

The standard deviation of linear distortion,  $(s_x, s_y, s_z, s_{xy}, s_{xz}, s_{yz})$ , was  $(0.27\%, 0.06\%, 0.03\%, 0.11^\circ, 0.37^\circ, 0.05^\circ)$  see Table 5. This shows that most of the measured distortion change applies to those components related to the  $x$  readout direction:  $(s_x, s_{xy}, s_{xz})$ . Figure 1 shows how  $(s_x, s_{xy}, s_{xz})$  change as a function of  $G_x$ . All decrease as  $G_x$  increases, the coefficient of linear correlation,  $r$ , for  $(s_x, s_{xy}, s_{xz})$  of  $(0.93, 0.87, 0.94)$ . The change in distortion for the various values of  $G_x$  relative to the standard FFE2 scan ( $G_x = 1.275\text{mT/m}$ ) corresponded to  $dp \leq 0.2\text{mm}$ . The  $dp_4$  measure was  $(32.94\%, 39.61\%, 5.60\%, 1.88\%)$  indicating that most of the measured distortion was either first or second order. For scans with  $G_x > 1.75$ , the scaling error in the readout direction ( $s_x$ ) increased as a function of readout gradient strength so these measurements were excluded from the analysis. There was high linear correlation between the  $dp(i)$  residual and  $G_x$  both before ( $r = 0.98$ ) and after ( $r = 0.98$ ) first order distortion correction.

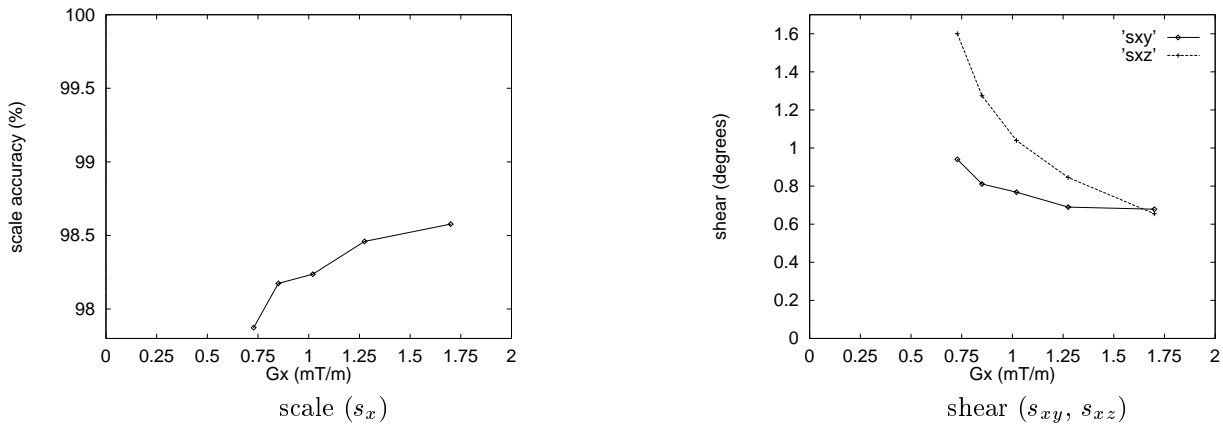


**Figure 1.** Scale ( $s_x$ ) and shear ( $s_{xy}, s_{xz}$ ) measurements in the readout direction as a function of the gradient strength,  $G_x$ , all measurements were with respect to the modelled reference structure locations (absolute).

### 4.3. Sequence parameters

For both FFE2 and SE sequences there was greatest variation in the readout dependent directions ( $s_x, s_{xy}, s_{xz}$ ). For the FFE2 sequence there was little change when TE was increased from 4.5 to 20 ms, there was, however, a larger change  $s_x$  (0.5%) and  $s_{xz}$  (0.5°) when TE was decreased from 4.5 to 3 ms – see Table 6. This change corresponded to a  $dp$  residual of 0.4mm. The mean sagittal shear,  $s_{xz}$ , was much larger for SE ( $-2.4^\circ$ ) compared to FFE2 ( $-0.92^\circ$ ). The two sets of  $s_{xz}$  shears were compared with the Wilcoxon rank sum test and this indicated that they were significantly different ( $p = 0.002$ ).

### 4.4. Shimming

It was noted that changing the shim setting from DS to AS produced changes in the FOV offset vector which resulted in translation. This was disregarded as translations do not affect distortion measurement, providing that the same reference structures are in the FOV. The largest distortion change for the FFE2 scans was for the AS and DS shim settings, this corresponded to a  $dp$  residual 1.2mm. The largest change in distortion components from AS to DS for both FFE1 and FFE2 was the sagittal shear  $s_{xz}$ . The change in the  $s_{xz}$  component of distortion for the FFE2 resulting from the different shim settings is illustrated in Figure 2. The  $s_{xz}$  shear change increased from  $-1.09^\circ$  (FFE1) to  $-2.13^\circ$  (FFE2). This change represents a doubling (1.97) of  $s_{xz}$  when the resolution and  $G_x$  are doubled. There was a similar pattern of increase for the corresponding MS to DS shim settings – see Table 7.

### 4.5. Distortion changes over time

For the time series of 11 FFE1 scans the mean (stdev) of the  $dp$  residual before distortion correction to the model was 1.02mm (0.04mm) and the corresponding maximum was 3.09mm (0.11mm). Figure 3 shows the change in linear distortion as a function of time. Both absolute and relative measurements are given and are plotted at the same scale to aid comparison. The mean accuracy of linear distortion ( $s_x, s_y, s_z, s_{xy}, s_{xz}, s_{yz}$ ) was (98.26%, 99.07%, 99.82%, 0.4°, 0.4°, 0.3°). There was little change over the 11 week period, the corresponding standard deviation was (0.09%, 0.04%, 0.06%, 0.02°, 0.05°, 0.03°). Table 8 compares the distortion measured with respect to the reference model and first scan in the time series.

### 4.6. Higher order distortion

The mean residual,  $dp(i)$ , for ( $n = 33$ ) FFE1, FFE2 and SE scans that were corrected to physical space decreased as a function of the polynomial order ( $r > 0.9, n = 33$ ). The corresponding  $dp_4$  measure was: (44.83%, 30.16%, 9.85%, 0.9%). This indicates that three-quarters of the distortion was either first or second order. To put this into a clinical context,  $dp_4$  was also determined for the time series of 11 FFE1 scans. These have similar sequence parameters and resolution as clinical serial MR images used in a recent growth hormone study.<sup>3</sup>  $dp_4$  was: (0.51mm, 0.27mm, 0.13mm, 0.01mm). Given that the threshold of discernible misregistration was about 200  $\mu\text{m}$  for

**Table 6.** Linear distortion as a function of the sequence parameters. Distortion was measured with respect to the modelled reference structures (absolute). The upper Table refers to the gradient echo sequence and the lower one to the spin echo one. For an explanation of the scan parameters see Table 2, page 3. The \* denotes that only 305 out of 427 balls were detected.

GRADIENT ECHO						
parameter	scale ( % )			shear (degrees)		
	$s_x$	$s_y$	$s_z$	$s_{xy}$	$s_{xz}$	$s_{yz}$
greSTD	98.43	99.46	99.84	0.63	1.03	0.16
greTR13	98.15	99.47	99.78	0.67	0.92	0.14
greTE3	98.91	99.45	99.85	0.53	0.56	0.14
greTE20*	98.44	99.40	99.54	0.51	1.05	0.05
greFA60	98.41	99.48	99.84	0.65	1.04	0.18
GRE Stats	$s_x$	$s_y$	$s_z$	$s_{xy}$	$s_{xz}$	$s_{yz}$
mean	98.47	99.45	99.77	0.60	0.92	0.14
std	0.28	0.03	0.13	0.07	0.21	0.05
SPIN ECHO						
parameter	$s_x$	$s_y$	$s_z$	$s_{xy}$	$s_{xz}$	$s_{yz}$
seSTD	98.16	99.41	100.46	0.34	-3.68	0.20
seTR200	98.31	99.46	100.15	0.30	-2.67	0.06
seTR1000	98.30	99.39	100.19	0.38	-2.65	0.16
seTE40	98.35	99.51	99.87	0.23	-1.29	0.16
seGap0.5	100.10	99.43	99.93	0.77	-1.78	0.06
SE Stats	$s_x$	$s_y$	$s_z$	$s_{xy}$	$s_{xz}$	$s_{yz}$
mean	98.65	99.44	100.12	0.40	-2.41	0.13
std	0.82	0.05	0.23	0.21	0.92	0.06

**Table 7.** Linear distortion change as a function of shim setting. Target image was with the default shim (DS) (relative).

Shim setting	scale ( % )			shear (degrees)		
	$s_x$	$s_y$	$s_z$	$s_{xy}$	$s_{xz}$	$s_{yz}$
autoslim FFE1	100.08	100.02	100.03	-0.04	-1.09	-0.02
autoslim FFE2	100.09	99.98	100.00	-0.12	-2.13	0.02
manual shim FFE1	100.25	99.97	99.86	-0.26	-0.43	0.03
manual shim FFE2	100.79	99.91	99.97	-0.42	-1.11	0.03

**Table 8.** Statistics for linear distortion measurements as a function of time. Measurements with respect to the modelled reference structure locations (upper Table) and with respect to the ones detected in the first scan of the series (lower Table).

ABSOLUTE MEASUREMENTS						
Statistic	scale (%)			shear (degrees)		
	$s_x$	$s_y$	$s_z$	$s_{xy}$	$s_{xz}$	$s_{yz}$
mean	98.26	99.07	99.82	0.39	0.42	0.26
std	0.04	0.03	0.06	0.02	0.07	0.02
RELATIVE MEASUREMENTS						
Statistic	$s_x$	$s_y$	$s_z$	$s_{xy}$	$s_{xz}$	$s_{yz}$
mean	100.02	100.01	100.05	-0.01	-0.01	-0.04
std	0.09	0.04	0.06	0.02	0.05	0.03

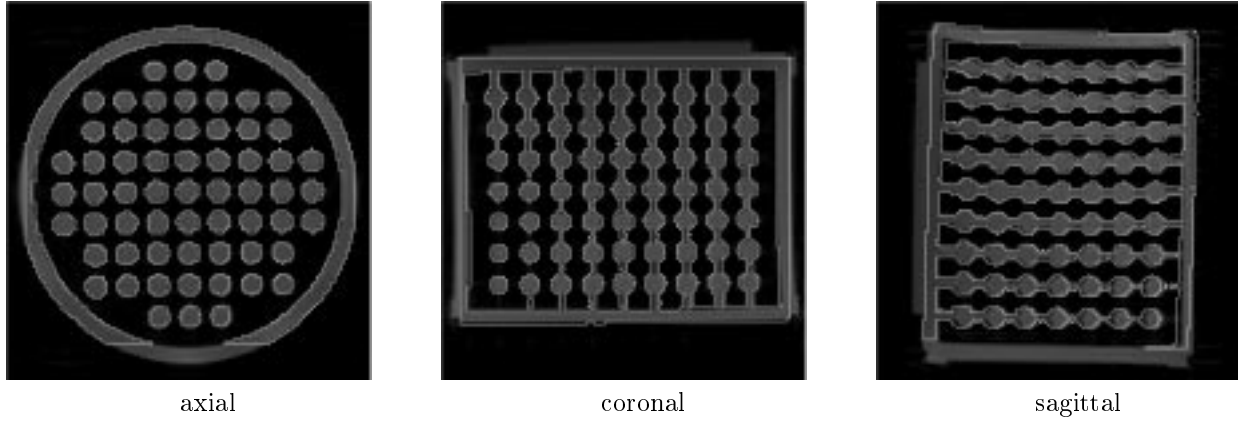


**Figure 2.** Changes in distortion for FFE2 scans as a function of the shim setting. The scan with the default shim setting (DS) is shown as a grey scale image and the one with the autoshim setting (AS) is shown as a threshold boundary in white. To compensate for a shift in offset vector introduced by shimming the AS scan was rigidly registered and sinc interpolated to the coordinate frame of the DS one. The largest geometrical difference is a sagittal shear change seen clearly in the sagittal view. The middle row of reference structures are in close correspondence and the upper and lower ones are shifted to the right and left.

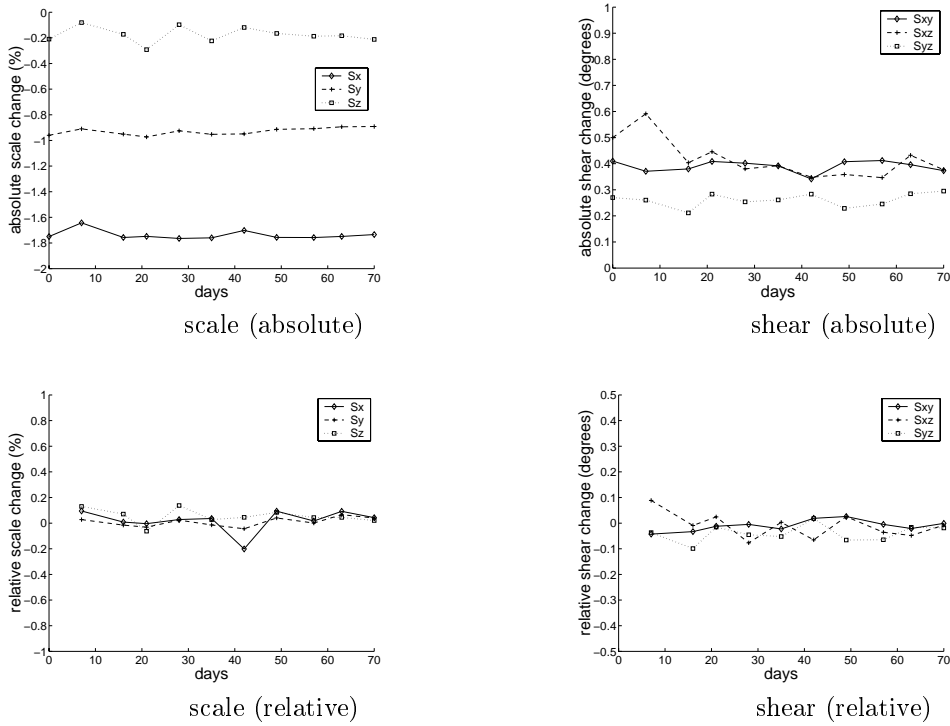


**Figure 3.** Change in linear distortion as a function of time. Top row refers to absolute measurements and the bottom row to measurements relative to the first scan in the time series.

**Table 9.** Distortion correction of brain images (FFE1). DS and MS refer to the default and manual shim settings.

shim settings		RMS of difference image (brain)	
source	target	no distortion correction	distortion correction
MS	DS	29.403	26.206

a similar sequence to FFE1<sup>9,3</sup> we can predict that third order polynomial correction is the most that is needed for serial MR applications with our Philips scanner.

#### 4.7. Correcting brain images for distortion change

The RMS of the difference image intensity is given in Table 9 and shows some improvement when distortion is corrected.

### 5. CONCLUSION

The distortion correction method assessed here produces consistent measurements of linear distortion when the phantom is repositioned by small amounts ( $s_x, s_y, s_z \leq 0.03\%$  ( $s_{xy}, s_{xz}, s_{yz} \leq 0.04^\circ$ ). The ( $s_x, s_{xy}, s_{xz}$ ) components of linear distortion showed a high degree of inverse correlation with readout gradient strength ( $r \geq 0.87$ ). There were significant differences in the  $s_{xz}$  component of distortion for the spin echo and 3D gradient echo images with the same resolution and readout gradient strength. This might be explained by the slice selection process which has frequency encoding in the through-slice direction – gradient errors also cause errors in the slice thickness and rotate slices with respect to each other.<sup>7</sup> Of the various parameters tested the shim setting had the greatest influence on distortion. Shimming produced large changes in linear distortion; these changes decreased as the scan resolution was increased. For a time series of weekly scans using a typical clinical MR sequence there was a negligible change in distortion over an 11 week period. Absolute measurements of the  $dp_4$  residual for these 11 scans indicated that three quarters of the distortion was either first or second order and that the benefit of third order correction was marginal and fourth order was unnecessary. Results for volunteer difference images showed that distortion correction reduced the amount of misregistration artefact, but probably insufficient to make it clinically useful. Phantom methods can only correct object independent distortion. To correct object dependent distortion the readout gradient reversal method by Chang and Fitzpatrick<sup>10</sup> is a strong candidate. However, intra-voxel dispersion is still an unsolved problem even with the improvements proposed by Kannengeisser et al.<sup>11</sup> This would, in particular, lead to errors at the tissue/air interface which would impede the detection of anatomical change in these regions, for example near the pituitary gland. An alternative option for applications that require to detect change in these regions might be to use the Sumanaweera method.<sup>5</sup>

### ACKNOWLEDGEMENTS

We would like to thank EasyVision Advanced Development, Philips Medical Systems for funding this work. We are grateful to Frans Gerritsen of his encouragement and constructive criticism. Kate McLeish would like to acknowledge EPSRC for funding her PhD studentship.

### REFERENCES

1. P. A. Freeborough, R. P. Woods, N. C. Fox, “Accurate Registration of Serial 3D MR Brain Images and its Application to Visualizing Change in Neurodegenerative Disorders,” *Journal of Computer Assisted Tomography* **20**(6), pp. 1012–1022, 1996.
2. L. Lemieux, G. Barker, “Measurement of small inter-scan fluctuations in voxel dimensions in magnetic resonance images using registration,” *Medical Physics* **25**(6), pp. 1049–1054, 1998.
3. M. Holden, E. R. E. Denton, J. M. Jarosz, T. C. S. Cox, D. J. Hawkes, D. L. G. Hill, “Detecting small anatomical change with 3D serial MR subtraction images,” in *Proceedings of Society of Photo-Optical Instrument Engineers (SPIE)*, **3661**, pp. 44–55, (San Diego), 1999.
4. M. Breeuwer, M. Holden, W. Zylka, “Detection and correction of geometric distortion in 3D MR images,” in *Proceedings of Society of Photo-Optical Instrument Engineers (SPIE)*, **4322**, (San Diego), 2001.

5. T. S. Sumanaweera, G. H. Glover, T. O. Binford, J. R. Adler, "MR Susceptability Misregistration Correction," *Transactions on Medical Imaging* **12**(2), pp. 251–259, 1993.
6. Z. P. Liang, P. C. Lauterbur, *Principles of Magnetic Resonance Imaging*, IEEE press, 2000. ISBN: 0-7803-4723-4.
7. E. M. Haacke, R. W. Brown, M. R. Thompson, R. Venkatesan, *Magnetic Resonance Imaging: Physical Principles and Sequence Design*, Wiley, 1999. ISBN: 0-471-35128-8.
8. M. Holden, D. L. G. Hill, E. R. E. Denton, J. M. Jarosz, T. C. S. Cox, T. Rohlfing, J. Goodey and D. J. Hawkes, "Voxel Similarity Measures for 3D Serial MR Brain Image Registration," *IEEE Transactions on Medical Imaging* **19**(2), pp. 94–102, 2000.
9. E. R. E. Denton, M. Holden, E. Christ, J. M. Jarosz, D. Russell-Jones, J. Goodey, T. C. S. Cox, D. L. G. Hill, "The identification of cerebral volume changes in treated growth hormone deficient patients using serial 3-D MR image processing," *Journal of Computer Assisted Tomography* **24**, pp. 139–145, January 2000.
10. M. Chang, M. J. Fitzpatrick, "A Technique for Accurate Magnetic Resonance Imaging in the Presence of Field Inhomogeneities," *IEEE Transactions on Medical Imaging* **11**(3), pp. 319–329, 1992.
11. S. A. R. Kannengiesser, S. I. Wang, E. M. Haacke, "Geometric distortion correction in gradient-echo imaging by use of dynamic time warping," *Magnetic Resonance in Medicine* **42**(5), pp. 585–590, 1999.